# Modulation instability, Cherenkov radiation and FPU recurrence

J. M. Soto-Crespo
*Instituto de Óptica, C.S.I.C., Serrano 121, 28006 Madrid, Spain*

A. Ankiewicz, N. Devine and N. Akhmediev
*Optical Sciences Group, Research School of Physics and Engineering, The Australian National University, Canberra ACT 0200, Australia*

We study, numerically, the influence of third-order dispersion (TOD) on modulation instability (MI) in optical fibers described by the extended nonlinear Schrödinger equation. We consider two MI scenarios. One starts with a continuous wave (CW) with a small amount of white noise, while the second one starts with CW with a small harmonic perturbation at the highest value of the growth rate. In each case, the MI spectra show an additional spectral feature that is caused by Cherenkov radiation. We give an analytic expression for its frequency. Taking a single frequency of modulation instead of a noisy CW leads to the Fermi-Pasta-Ulam (FPU) recurrence dynamics. In this case, the radiation spectral feature multiplies due to the four-wave mixing process. FPU recurrence dynamics is quite pronounced at small values of TOD, disappears at intermediate values and is restored again at high TOD when the Cherenkov frequency enters the modulation instability band. Our results may lead to a better understanding of the role of TOD in optical fibers.

## I. INTRODUCTION

Third-order dispersion (TOD) plays an important role in optical wave propagation in optical fibers. TOD is the origin of the generation of Cherenkov radiation by solitons [1]. It serves as a seeding source for super-continuum generation in optical fibres pumped by continuous waves [2]. It causes the emission of optical rogue waves [3, 4]. It is also the reason for the amplification of strong solitons at the expense of weak ones [5]. There have been quite a few theoretical and experimental works devoted to the study of third-order dispersion and its influence on solitons [6–8]. Recently, Droques *et al.* [9] undertook an experimental investigation of modulation instability in the presence of TOD. They observed symmetry-breaking of the MI spectrum in optical fibers, and, more importantly, an additional spectral feature that appears in otherwise-typical MI spectra. This is a new phenomenon that the authors confirmed numerically. However, the nature of this spectral feature still needs a solid theoretical background and physical explanations. Such explanations are provided in our present work.

Modulation instability (MI) is an interesting and rich phenomenon that has attracted the attention of scientists in various fields again and again [10–17]. This subject has usually been addressed in two different ways. In one case, modulation instability develops from a noisy background when the initial condition is a CW with a perturbation that contains all possible frequencies of modulation. Then the initial stage of evolution is dominated by the component with the largest growth rate. However, all other frequencies also grow, although at a slower pace [18]. The resulting widening of spectra is the first step for super-continuum generation in optical fibers. The second approach to this challenge consists of perturbing the initial CW with a single frequency of modulation. When solving this problem, fundamental phenomena like FPU recurrence [19, 20] and sophisticated higher-order MI effects [21, 22] have been revealed.

Clearly, the question of how TOD influences each of these two regimes also has to be split into two parts. In this work, we consider each case separately, in order to build a complete picture of the influence of TOD on modulation instability. Such a complex approach has allowed us to reveal new and unexpected ways of how TOD influences the evolution of waves that start with the standard MI.

## II. BASIC EQUATIONS

The most common dimensional form of the nonlinear Schrödinger equation (NLSE) for waves in optical fibers close to the zero dispersion point is [23–25]

$$i\Psi_Z - \frac{\beta^{(2)}}{2}\Psi_{TT} + \frac{n_2\omega_0}{c}|\Psi|^2\Psi = i\frac{\beta^{(3)}}{6}\Psi_{TTT}, \qquad (1)$$

where $\Psi$ is the amplitude of the slowly-varying envelope of the optical field, $\beta^{(n)}$ is the n-th order dispersion parameter [i.e., $\beta^{(n)} = \partial^n\beta/\partial\omega^n$ evaluated at the carrier frequency $\omega_0$], $n_2$ is the nonlinear index of refraction while $c$ is the speed of light.

By using the transformation:

$$z = Z/\lambda, \qquad t = T/\sqrt{\lambda}, \qquad \psi = \sqrt{n_2/(2\pi)}\Psi, \qquad (2)$$

where $\lambda$ is the wavelength, Eq.(1) can be reduced to its normalized form

$$i\psi_z + \frac{\beta_2}{2}\psi_{tt} + |\psi|^2\psi = i\beta_3\psi_{ttt}, \qquad (3)$$

where

$$\beta_2 = -\beta^{(2)}, \qquad \beta_3 = \frac{\beta^{(3)}}{6\sqrt{\lambda}} \qquad (4)$$

When $\beta_3$ is zero, equation (3) becomes the standard NLSE, which is integrable. Reversing the transformations (2) we can always return to dimensional units.

The continuous wave (CW) solution of Eq.(3) is

$$\psi = Ae^{iA^2 z} \tag{5}$$

Without loss of generality, we can take $A = 1$, as we can always use the scaling transformation [8] to return to an arbitrary amplitude.

In the absence of TOD, and for positive $\beta_2$, equation (3) has a family of solutions that are presently known as Akhmediev breathers (AB) [26, 27]. By choosing $\beta_2 = 1$ without losing any generality, they are given by

$$\psi(t,z) = \left[1 - \frac{\frac{\Omega^2}{2}\cosh(\delta z) + i\delta\sinh(\delta z)}{\cosh(\delta z) - \frac{\delta}{\Omega}\cos(\Omega t)}\right]\exp(iz). \tag{6}$$

This equation defines a family of solutions. The free parameter of the family is $\Omega$; it varies in an interval between 0 to 2 and defines the frequency of the initial modulation $\Omega$ and the initial growth rate of the modulation:

$$\delta = \Omega\sqrt{1 - \frac{\Omega^2}{4}}.$$

When $z \to \pm\infty$, this solution becomes the plane wave $e^{iz+i\phi}$ with different phases $\phi$ at the two limits. Taking into account the lowest-order modulated terms, Eq.(6) can be approximated at $z \to -\infty$ by

$$\psi(t,z) = \left[1 - \mu\delta\left(\Omega + i\frac{2\delta}{\Omega}\right)e^{\delta z}\cos(\Omega t)\right]e^{iz+i\phi}, \tag{7}$$

where $\mu$ is a small real parameter and $\phi$ is the initial phase of the CW. The exponential factor $e^{\delta z}$ in (7) clearly shows that the solution (6) starts from modulation instability. Using (7) as the initial condition in simulating wave propagation, we can recover the solution (6). Ignoring the complex factor when taking a small amplitude $\mu$ shifts the simulations from the exact heteroclinic orbit to a nearby periodic solution. We note that there is a nonlinear phase shift related to recurrence [28] which makes the trajectory heteroclinic rather than homoclinic.

The discrete spectral components of (6) evolve according to [6, 18]:

$$A_0(z) = 1 - \frac{i\delta\sinh(\delta z) + (\Omega^2/2)\cosh(\delta z)}{\sqrt{\cosh^2(\delta z) - \frac{\delta^2}{\Omega^2}}} \tag{8}$$

$$A_n(z) = \frac{i\delta\sinh\delta z + (\Omega^2/2)\cosh(\delta z)}{\sqrt{\cosh^2(\delta z) - \frac{\delta^2}{\Omega^2}}} \times \left[\Omega\frac{\cosh(\delta z) - \sqrt{\cosh^2(\delta z) - \frac{\delta^2}{\Omega^2}}}{\delta}\right]^{|n|} \tag{9}$$

where $\Omega$ and $\delta$ are the same as above. On a logarithmic scale, the spectrum has a triangular shape [18], though we must remember that it is discrete.

An interesting question has been raised in the recent work of Mahnke and Mitschke [26]. Namely, how stable are ABs relative to various perturbations? The authors have found that perturbations of the wave field governed by the NLSE do not destroy ABs. On the other hand, perturbing the NLSE with a small Raman term splits ABs into solitons - a process which is an essential part of super-continuum generation in fibers. Generally speaking, other perturbations that lift integrability of the NLSE should lead to similar dynamics. TOD would be one of these perturbations. However, the influence of TOD is more complicated, as we can see from our simulations presented below. In order to see these complications, we have to look deeper into the mechanism of radiation.

## III. RESONANT RADIATION AND ITS FREQUENCY

It is well-known that TOD creates radiation waves [1]. Generally, only $t$-dependent solutions produce radiation. A CW solution by itself does not produce radiation waves. They appear only when the CW is split into separate pulses according to (6). As a result, we can view small amplitude radiation waves as being generated just as occurs in the soliton case. Here, we use the NLSE in the form given by Eq.(3). Then, we can represent dispersive waves in the form

$$\psi = \mu e^{i(kz-\omega t)}, \tag{10}$$

where $\mu$ is a small amplitude and $k$ is the propagation constant. The frequency then satisfies the dispersion relation

$$-k - \omega^2\beta_2/2 = -\beta_3\omega^3 \tag{11}$$

In order for this radiation to be resonant with the AB solution which serves as the source of the radiation, its propagation constant should coincide with that of the AB. This is a condition for Cherenkov radiation and it is given by $k = A^2 = 1$.

Thus, the condition for the resonance is

$$A^2 = 1 = -\omega^2\beta_2/2 + \beta_3\omega^3, \tag{12}$$

and we have the following cubic equation to solve:

$$\omega^3 - \frac{\beta_2}{2\beta_3}\omega^2 - \frac{1}{\beta_3} = 0. \tag{13}$$

Eq.(13) can be solved analytically [29]. For positive $\beta_2$, among the three roots, two are complex conjugates and one is purely real. The sign of the real root coincides with the sign of $\beta_3$. This real solution

$$\boxed{\omega = \frac{\chi^2 + \beta_2\chi + \beta_2^2}{6\beta_3\chi}} \tag{14}$$

where $\chi = \left(\beta_2^3 + 108\beta_3^2 + 6\sqrt{6}\sqrt{\beta_2^3\beta_3^2 + 54\beta_3^4}\right)^{1/3}$ provides us with the resonant condition for dispersive linear waves created by an AB. Despite being only an approximation, our simulations presented below show that the resonant frequency is accurately fitted by this equation.

The numerical simulations are done by solving Eq.(3) with initial conditions consisting of a constant amplitude field plus small complex amplitude white noise. To be precise:

$$\psi(z=0,t) = 1 + a(t) + ib(t), \tag{15}$$

where $a(t)$ and $b(t)$ are two uncorrelated real random functions which take values uniformly distributed in a small interval around 0. This initial condition leads to modulation instability within the instability band so that the sidebands inside the gain bandwidth, i.e. for $|\omega| < 2$, increase their amplitudes exponentially during the initial stages of propagation according to (7). We have chosen the propagation distance to be $z = 20$, which corresponds to a short fiber, so that the spectral component that has the highest growth rate dominates the evolution. Logically, for each realization, when using specific values of the random functions $a$ and $b$, and for fixed propagation distance, the spectrum appears to be noisy. In order to have uniform results, we have averaged the output spectra for a minimum of 100 different realizations. Then the average output spectra are smooth, and the simulations can mimic actual experiments undertaken in ([9]).

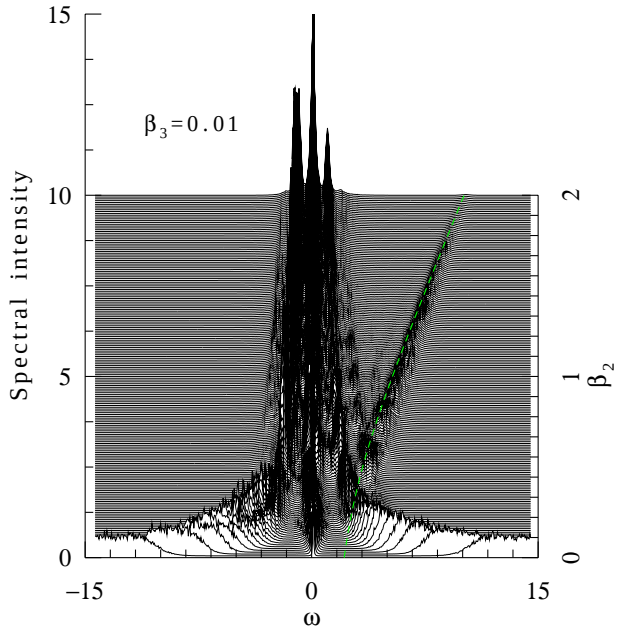


FIG. 1. (Color online) Spectral output intensity for a propagation distance $z = 20$, $\beta_3 = 0.01$ and for various values of $\beta_2$. The two sidebands are related to modulation instability, while the additional spectral band on the right represents the resonant radiation. The green dashed line, defined by Eq.(14), is in perfect agreement with the numerical simulations.

Here, we are interested in the average spectral output of the optical fiber versus the dispersion coefficients. Such data would describe the type of experiment presented in [9]. Figure 1 shows the shapes of the spectra at an early fixed stage of MI evolution for various values of $\beta_2$. The value of $\beta_3 = 0.01$ here is taken to be small and fixed. The total propagation distance is also fixed at $z = 20$. The spectral component, additional to the standard MI sidebands, that appears on the right-hand-side of the spectra in Fig.1 is caused by TOD, and is well-approximated by Eq.(14). The latter is shown by the green dashed curve. As we can see from this figure, the location of the resonant frequency is perfectly described by this simple result. Our theory is also in agreement with the numerical and the experimental results of the work [9]. Note that the axis of $\beta_2$ of Figures 1 and 2 of [9] is inverted - the value of $\beta_2$ grows downwards, which is opposite to our choice.

Another set of data is presented in Figure 2. Here, we have kept the value of $\beta_2 = 1$ constant while $\beta_3$ is changed from 0 to 1. The resonant frequency of dispersive waves is seen on the right-hand-side of the spectrum. It approaches the MI sideband monotonically while $\beta_3$ grows from 0 to 1. The calculation giving the white dashed curve is based on Eq.(14). It approximates reasonably well the spectral feature caused by the dispersive waves at small values of $\beta_3$ when the MI evolves according to the unperturbed NLSE. Higher values of $\beta_3$ significantly influence the basic process of MI.

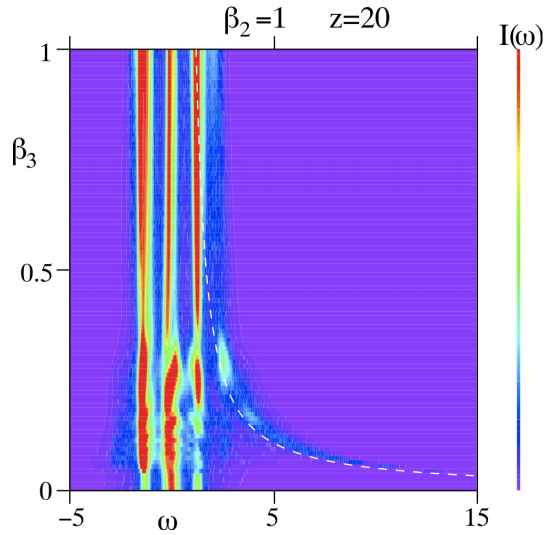


FIG. 2. (Color online) Spectral intensity output of the fiber for a propagation distance of $z = 20$ and $\beta_2 = 1$, as a function of $\beta_3$. The white dashed line is given by Eq.(14).

## IV. INFLUENCE OF RADIATION ON FPU RECURRENCE

The influence of dispersive waves on the MI spectra is clearly seen at small propagation distances. What will happen when the distances increase? FPU recurrence was observed experimentally by Van Simaeys *et al.* in [19]. Will it also be seen here? Preliminary studies in this regard have been carried out in [6]. Here, we give a more detailed answer to the above question.

It is well-known that modulation instability in the NLSE, when started with a single sideband, results in recurrence. This is called Fermi-Pasta-Ulam recurrence: the dynamical system returns to the same state of single mode excitation from which the dynamics started. This process is perfectly described by the AB solution (6) [20, 28]. Observation of the FPU recurrence requires more accurate initial conditions than in (15). We have to use strictly periodic initial conditions like (7), rather than CW with a random perturbation. Thus, as initial conditions in the numerical simulations below, we took a constant amplitude field, slightly modulated with a frequency $\omega$ located within the instability band:

$$\psi(z=0,t) = 1 + \mu\cos(\omega t), \tag{16}$$

where $\mu$ is a small constant. With this initial condition and $\mu$ complex, as in (7), and with $\beta_3 = 0$, the field governed by the NLSE evolves according to Eq.(6). Deviations from the exact initial conditions, such as taking $\mu$ to be real instead of complex, results in a deviation from the exact heteroclinic trajectory, thus producing periodic evolution. In the following simulations we use small $\mu = 0.0001$, and $\omega = \sqrt{2}$. This frequency produces the highest MI gain for a field amplitude 1. Here, and in the rest of the paper, we assume $\beta_2 = 1$.

Now, we turn to the case of nonzero $\beta_3$. Figure 3 shows the spectrum evolution of the solution that starts with the initial condition (16). For a small value of $\beta_3$ (=0.01), the solution is close to (6) with a spectrum close to that defined in (8). The first expansion of the spectrum at $z \approx 10$ is indeed very close to the analytic expression. The spectrum starts to evolve periodically as the heteroclinic orbit is transformed to periodic motion for any small perturbation. A small amplitude spectral feature, corresponding to the dispersive waves, is clearly seen on the right-hand-side of the spectrum. The value of the radiation frequency is indeed given by the resonant condition (14). It is indicated by the blue dashed vertical line in this figure. The radiation component grows during propagation, as some is emitted each time when the optical field splits into pulses. For the small value of $\beta_3$ considered in this example, the influence of radiation on the AB is almost negligible. Thus, recurrence to the plane wave occurs for many periods of evolution. Three of them can be seen in Figure 3, and periodic evolution continues well after $z = 50$.

For higher values of $\beta_3$ the recurrence is restricted to only a few cycles. Increasing $\beta_3$ up to 0.02 firstly leads to

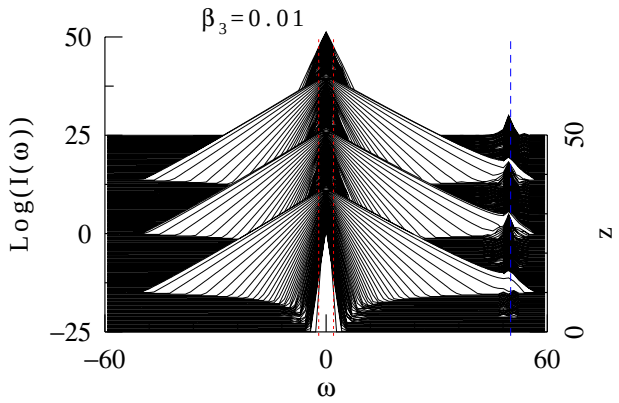


FIG. 3. (Color online) Recurrence spectrum of the NLSE with small TOD, namely $\beta_3 = 0.01$, while $\beta_2 = 1$. The TOD resonant radiation can be seen on the right-hand-side of the spectrum. Its position is indicated by the dashed blue line. Its influence is negligible until the radiation grows to higher amplitudes and distorts the initially symmetric AB spectrum. However, this distortion occurs at very long propagation distances. The two red vertical lines show the limits of the modulation instability region ($\pm 2$). The initial condition contains only a single pair of sidebands at the maximum growth rate ($\omega = \sqrt{2}$. The periodicity is preserved on propagation by imposing periodic boundary conditions, such that the whole spectrum remains discrete. The discreteness cannot be seen on this plot and in the plots below, since the curves are drawn by joining the discrete spectrum values with straight lines.

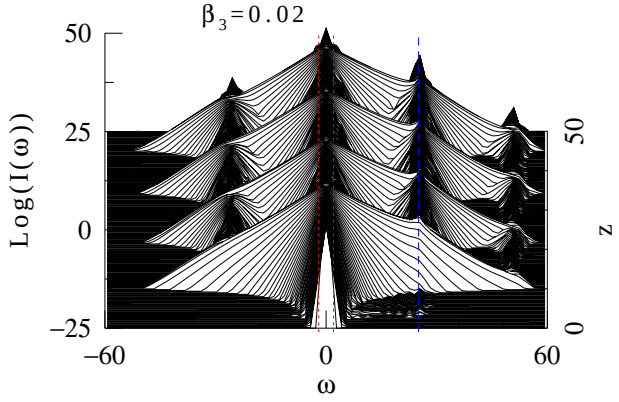


FIG. 4. (Color online) The same as in Fig.3, except that the TOD is higher: $\beta_3 = 0.02$. According to Eq.(14), TOD resonant radiation is now closer to the pump. It hardly influences the first recurrence, but due to the four-wave mixing (FWM) process through the pump, the resonant radiation appears almost symmetrically on the left-hand-side of the spectrum. Moreover, an additional "sideband" of the resonant radiation appears at an equal distance on the right-hand-side of the spectrum. The asymmetry between the l.h.s. and r.h.s of the spectrum is due to the delay in the transfer of the spectral energy to the left-hand-side of the spectrum. The influence of the radiation is stronger than in the previous case, as the radiation appears on top of stronger spectral components. The radiation accumulates faster and recurrence survives shorter distances. Four cycles of recurrence can be seen here.

the shift of the resonant frequency, which becomes closer to the pump frequency. Secondly, it leads to the intensity increase of the radiation waves. The results are shown in Fig.4. Another significant difference from the previous case is that the resonant radiation also appears on the left-hand-side of the spectrum due to the four-wave-mixing (FWM) process. These radiation components of the spectrum are repeated at equal spectral intervals on the left and right-hand-sides of the initial resonant frequency. The latter is indicated by the vertical dashed blue line. As a result, we obtain an equi-distantly located comb of dispersive spectral components on top of the original AB spectrum, with amplitudes that grow continuously, but very slowly. These components are hardly visible at the first appearance of the triangular AB spectrum, but they significantly disturb the triangular spectra repeatedly appearing in the subsequent evolution. The level of disturbance is still small for $\beta_3 = 0.02$, and clear FPU recurrence can be observed at least four times in this figure. The period in $z$ is reduced here due to a higher level of deviation from the heteroclinic trajectory.

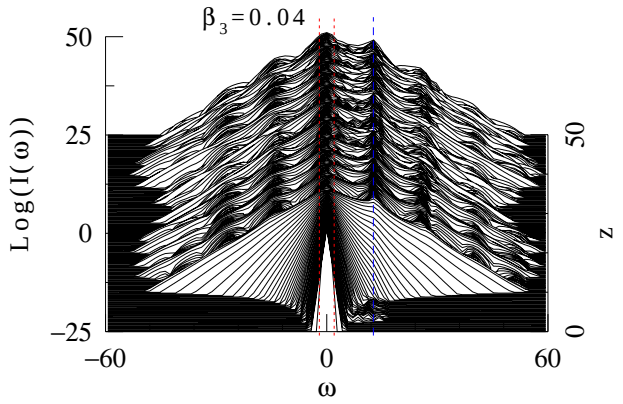


FIG. 5. (Color online) The same as in Figs.3 and 4, except that the TOD is further increased to $\beta_3 = 0.04$. TOD resonant radiation (shown by the blue dashed line) is now much closer to the pump, but is still out of the instability band shown by the red dashed lines. The four-wave mixing process through the pump adds distortions on each side of the spectrum. The resonant radiation appears at higher values of the background spectrum, thus increasing its influence. It accumulates much faster and FPU recurrence is lost right from the first broadening of the spectrum. No cycles of recurrence can be seen here.

A further increase of $\beta_3$ to 0.04 leads to dispersive spectral features being even closer to the pump frequency. This is clearly seen in Fig.5. The first expansion of the spectrum is close to the AB spectrum. Further evolution is greatly influenced by the FWM of the pump and radiation. Higher amplitudes of radiation waves result in the complete loss of FPU recurrence after the first cycle. The spectra evolve irregularly, though they retain a roughly triangular shape, with the dispersive comb still being visible for short distances of propagation.

The above results are summarized in Fig.6. It shows the evolution of the peak amplitude, which occurs at $t = 0$, for the initial condition given by Eq.(16) for three values of $\beta_3$ used in the simulations. In all three cases, the initial stage of evolution is an exponential growth of the perturbation, just as the AB solution predicts. Consequently, the three curves almost coincide up to $z = 12$. When $\beta_3 = 0.02$, the following evolution of the peak amplitude shows almost perfect periodic behavior, demonstrating four clear recurrences up to the distance $z = 50$. Much better recurrence evolution can be observed at smaller values of $\beta_3$ ( not shown here). At higher values of $\beta_3$ (say 0.03), the recurrence is still observable, but it becomes less regular. The value $\beta_3 = 0.04$ is critical (blue dashed curve). In this case, the peak amplitude follows the recurrence trend only once. The subsequent evolution becomes completely irregular.

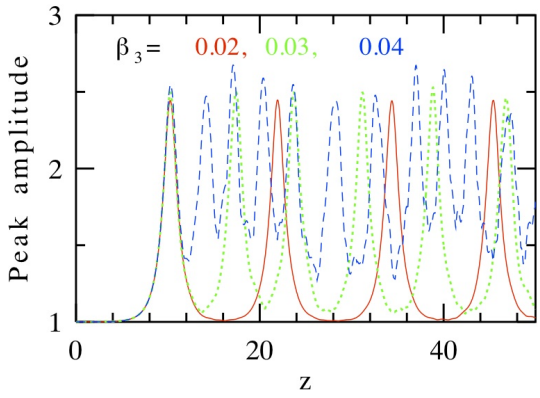


FIG. 6. (Color online) Field evolution, starting with modulation instability, for three small values of TOD. The solid red curve is for $\beta_3 = 0.02$, the green dotted line is for $\beta_3 = 0.03$, and the blue dashed curve for $\beta_3 = 0.04$. Up to $z = 12$, the three curves almost coincide. Multiple recurrence is clearly seen at the initial stages of evolution for the smallest values of $\beta_3$. Increasing the value of the TOD parameter causes the periodic behavior to deteriorate.

## V. RECOVERY OF FPU RECURRENCE AT HIGHER VALUES OF $\beta_3$

There are two characteristic frequencies in this problem. One is the upper limit of modulation instability and the second is the resonant frequency. Looking at Fig.2, we can find that the resonant frequency enters the MI instability band $\omega = 2$ at around $\beta_3 = 0.4$. We can expect that the MI dynamics will drastically change at that point. Amazingly, the FPU recurrence is completely restored above $\beta_3 = 0.4$. This happens because the resonant frequencies enter modulationally unstable dynamics, rather than evolving as independent components. Instability within the MI band completely dominates the growth of radiation waves. Figure 7 shows the spectral

evolution when $\beta_3 = 1.0$. We can clearly see the three growth-return cycles of the MI dynamics up to a distance of just $z = 50$. Periodic dynamics is repeated for much larger distances.

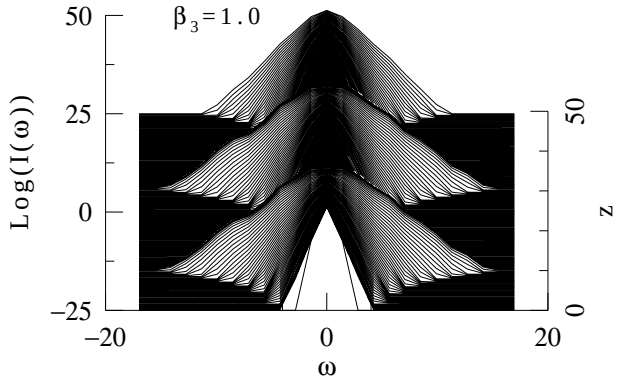


FIG. 7. (Color online) FPU recurrence dynamics of MI with almost perfect triangular spectrum of the sidebands when $\beta_3 = 1.0$. The resonant frequency here is within the MI band. It defines the fundamental frequency of the sidebands.

Figure 8 resumes our observations. When $\beta_3 = 0.3$, the dynamics is chaotic (red curve). The resonant frequency here is still out of the instability band. For the values $\beta_3 = 0.4$ (green dashed curve) and $\beta_3 = 0.5$ (blue dashed curve), the resonant frequency enters the instability band and we can see increasingly improved FPU recurrence dynamics as $\beta_3$ increases, at least up to a distance of $z = 50$. Generally, there is no qualitative reason for FPU dynamics to stop above these values. Our simulations with $\beta_3$ increasing indefinitely still show perfect recurrence.

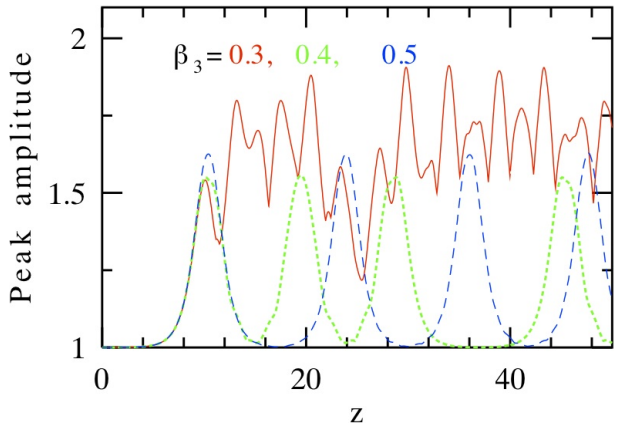


FIG. 8. (Color online) Optical field evolution, starting with modulation instability for three larger values of TOD: the red solid line stands for $\beta_3 = 0.3$, the green dotted line for $\beta_3 = 0.4$ and the dotted blue line for $\beta_3 = 0.5$. Recurrence, which was lost for small values of $\beta_3$, starts to be seen again for larger values of TOD, namely for $\beta_3 > 0.3$.

Figure 9 shows the evolution of the MI sidebands when $\beta_3 = 1.0$. As we can see, after the first cycle of recurrence dynamics, the sidebands disappear until the second cycle. This is a clear indication of the FPU recurrence process. All the energy returns to the pump frequency between the cycles. The trajectories in this process of dynamics are much closer to the heteroclinic ones than at lower values of $\beta_3$. The general conclusion is that, with $\beta_3$ increasing above 0.4, the FPU recurrence is recovered. In this sense, TOD has physics that is different from that of the Raman effect in the studies of Mahnke and Mitschke [26].

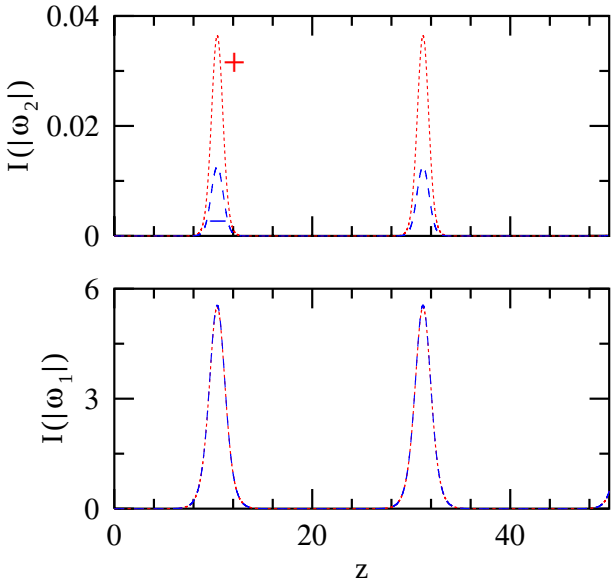


FIG. 9. (Color online) Evolution of the two nearest sidebands, $\pm\omega_1$ and $\pm\omega_2$, in the MI recurrence dynamics at $\beta_3 = 1.0$. The plus (red curves) and minus (blue curves) signs denote the r.h.s. and l.h.s. sidebands, respectively. The first sidebands (b) are almost symmetric while the second sidebands (a) have significant amount of asymmetry.

To further confirm the above conclusion, we have constructed trajectories in the complex plane of the solution. Figure 10 shows the recurrent feature of the trajectories on the complex plane of $\psi(z,t)$ for three values of $\beta_3$. As expected, at low values of $\beta_3$, (red curve) the trajectory is close to the original one, defined by the AB solution (green curve). Only the case of the maximum growth rate is shown here. At a high value of $\beta_3$ the trajectory (blue curve) becomes qualitatively different, but remarkably it is also recurrent. In order to prevent rotation of the trajectories in the complex plane, the propagation constant $q$ in the exponential has been shifted to the new value shown in this figure.

## VI. CONCLUSIONS

In conclusion, we have studied the influence of TOD on modulation instability of CW solutions of the NLSE. We have shown that, for a randomly perturbed CW,

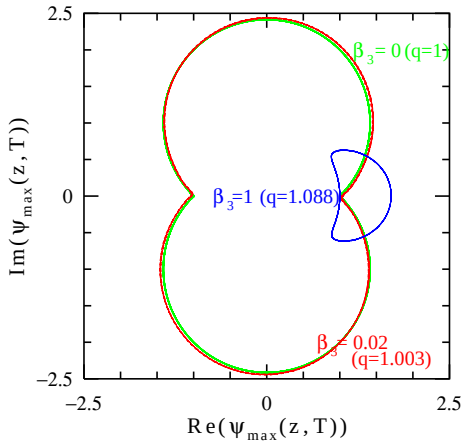


FIG. 10. (Color online) Recurrent trajectories of MI dynamics for $\beta_3 = 0$ (green curve), $\beta_3 = 0.02$ (red curve) and $\beta_3 = 1$ (blue curve).

TOD results in resonant radiation waves caused by the Cherenkov effect, and we have obtained a very good estimate of the frequency of this radiation. On the other hand, when the CW is perturbed with a single frequency, the radiation is multiplied due to the four-wave mixing effect. This causes the normally-recurrent solution to be converted into an aperiodic one. An interesting finding is that the periodicity is improved and the radiation disappears at higher values of the TOD coefficient, when the resonant frequency enters the modulation instability band.

The first part of our results have been observed in the experimental work of Droques *et al.* [9], and here we have given the theoretical background for these fascinating observations, as well as supplying the frequency of the additional peak in the spectra. Clearly, these estimates can be used for extracting the parameters of the fiber from experimental data. The second part of our results awaits future exciting experimental observations. These observations can be made at frequencies close to the zero dispersion point of the fiber, where TOD is comparable to second-order dispersion.

## ACKNOWLEDGMENTS

The work of J.M.S.C. is supported by the MINECO under contract FIS2009-09895. The authors acknowledge the support of the Australian Research Council (Discovery Project number DP110102068). N.A. is a recipient of the Alexander von Humboldt Award.

[1] N. Akhmediev and M. Karlsson, Cherenkov radiation emitted by solitons in optical fibres, Phys. Rev., **51**, 2602 (1995).
[2] J. M. Dudley, G. Genty, F. Dias, B. Kibler, N. Akhmediev, Modulation instability, Akhmediev Breathers and continuous wave supercontinuum generation, Opt. Express, **17**, 21497 (2009).
[3] M. Taki, A. Mussot, A. Kudlinski, E. Louvergneaux, M. Kolobov, M. Douay, Third-order dispersion for generating optical rogue solitons, Physics Letters A **374** 691695 (2010).
[4] G. Genty, C. M. de Sterke, O. Bang, F. Dias, N. Akhmediev, J. M. Dudley, Collisions and turbulence in optical rogue wave formation, Physics Letters A **374**, 989996 (2010).
[5] N. Akhmediev, J.M. Soto-Crespo, and A. Ankiewicz, Could rogue waves be used as efficient weapons against enemy ships?, Eur. Phys. J. Special Topics **185**, 259266 (2010).
[6] N. N. Akhmediev, V. I. Korneev, and N. V. Mitskevich, Modulation instability of a continuous signal in an optical fibre taking into account third order dispersion, Izvestiya Vysshikh Uchebnykh Zavedenii, Radiofizika, Vol. 33, pp. 111-117, (1990).
[7] M. I. Kolobov, A. Mussot, A. Kudlinski, E. Louvergneaux, and M. Taki, Third-order dispersion drastically changes parametric gain in optical fiber systems, Phys. Rev. A **83**, 035801 (2011).
[8] N. Akhmediev and A. Ankiewicz, "Solitons: nonlinear pulses and beams", Chapman & Hall, London, 1997.
[9] M. Droques, B. Barviau, A. Kudlinski, M. Taki, A. Boucon, T. Sylvestre, and A. Mussot, Symmetry-breaking dynamics of the modulational instability spectrum, Opt. Lett., **36**, 1359 (2011).
[10] V. I. Bespalov and V. I. Talanov, Filamentary structure of light beams in nonlinear liquids, JETP Lett. 3, 307-310, (1966)
[11] T. B. Benjamin and J. E. Feir, The disintegration of wavetrains on deep water. Part 1: Theory, J. Fluid Mech. 27, 417-430 (1967).
[12] G. P. Agrawal, Modulation Instability Induced by Cross-Phase Modulation, Phys. Rev. Lett., **59**, 880 (1987).
[13] D. Kip, Marin Soljacic, M. Segev, E. Eugenieva, D. N. Christodoulides, Modulation Instability and Pattern Formation in Spatially Incoherent Light Beams, Science, **290**, 495 (2000).
[14] A.V. Gorbach, X. Zhao, and D.V. Skryabin, Dispersion of nonlinearity and modulation instability in sub-wavelength semiconductor waveguides, Optics Express, **19**, 9345 (2011).
[15] K. Porsezian, K. Senthilnathan and S. Devipriya, Modulation instability in Fiber Bragg grating with non-Kerr nonlinearity, IEEE J. Quant. Electron., **41**, 789 (2005).
[16] N. C. Panoiu, X. F. Chen, and R. M. Osgood, Modulation instability in silicon photonic nanowires, Opt. Lett. **31**, 3609 - 3611 (2006).
[17] K. Kasamatsu and M. Tsubota, Modulation instability and solitary-wave formation in two-component Bose-Einstein condensates, Phys. Rev. A **74**, 013617 (2006).

[18] N. Akhmediev, A. Ankiewicz, J. M. Soto-Crespo and J. M. Dudley, Universal triangular spectra in parametrically-driven systems, Phys. Lett., **375**, 775 (2011).

[19] G. Van Simaeys, Ph. Emplit and M. Haelterman, Experimental demonstration of the Fermi-Pasta-Ulam recurrence in a modulationally unstable optical wave, Phys. Rev. Lett. **87**, 033902 (2001).

[20] N. Akhmediev, *Deja vu in optics*, Nature, **413**, No 6853, pp. 267 - 268 (2001).

[21] S. Wabnitz and N. Akhmediev, Efficient modulation frequency doubling by induced modulation instability, Opt. Commun. **283**, 1152 (2010).

[22] M. Erkintalo, K. Hammani, B. Kibler, C. Finot, N. Akhmediev, J. M. Dudley, and G. Genty, Higher-Order Modulation Instability in Nonlinear Fiber Optics, Phys. Rev. Lett., **107**, 253901 (2011).

[23] M. J. Potasek, Modulation instability in an extended nonlinear Schrodinger equation, Opt. Lett., **12**, 921 (1987).

[24] K. Tai, A. Hasegawa, and A. Tomita, Observation of Modnlational Instability in Optical Fibers, Phys. Rev. Lett., **56**, 135 (1986).

[25] Solange B. Cavalcanti, Jose C. Cressoni, Heber R. da Cruz, and Artur S. Gouveia-Neto, Modulation instability in the region of minimum group-velocity dispersion of single-mode optical fibers via an extended nonlinear Schrodinger equation, Phys. Rev. A **43**, 6162 (1991).

[26] Ch. Mahnke and F. Mitschke, Possibility of an Akhmediev breather decaying into solitons, Phys. Rev. A **85**, 033808 (2012).

[27] M. Erkintalo, G. Genty, B. Wetzel, J. M. Dudley, Akhmediev breather evolution in optical fiber for realistic initial conditions, Phys. Lett., A **375**, 2029 (2011).

[28] N. Devine, A. Ankiewicz, G. Genty, J.M. Dudley, N. Akhmediev, Recurrence phase shift in FermiPastaUlam nonlinear dynamics, Phys. Lett. A, **375**, 4158 - 4161 (2011).

[29] M. Abramowitz and I. A. Stegun, Handbook of mathematical functions with formulas, graphs and mathematical tables, (Dover publications, NY, 1972).